International Journal of Nanoelectronics and Materials
Volume 16 (Special Issue) December 2023 [221-239]

Characterization and Kinetic Study of TiO_2/ ZnO Co-Doped with Nitrogen and Sulphur at Different Calcination Temperature

Nur Najwa Yunus[1], Fazlena Hamzah[1,*], Mohamad Sufian So'aib[2], and Jagannathan Krishnan[3]

[1]Biocatalysis and Biobased Material Technology Research Innovative Group, School of Chemical Engineering, College of Engineering, Universiti Teknologi MARA, UiTM Shah Alam, 40450 Shah Alam, Selangor, Malaysia
[2]School of Chemical Engineering, College of Engineering, Universiti Teknologi MARA, UiTM Cawangan Pulau Pinang, Kampus Permatang Pauh, 13500 Bukit Mertajam, Pulau Pinang, Malaysia
[3]Department of Chemical Engineering, SSN College of Engineering, Kalavakkam, 603110, India

ABSTRACT

TiO_2/ZnO nanocomposites, have garnered significant attention for their potential applications in environmental remediation and sustainable energy production. Doping these materials with non-metals like nitrogen and sulphur and using optimum calcination temperature holds promise for enhancing their photocatalytic efficiency. However, a comprehensive investigation into the impact of calcination temperature on nitrogen and sulphur co-doped TiO_2/ZnO nanocomposites remains relatively unexplored and limits their extensive use in photocatalysis and makes it difficult to customise the materials for particular purposes. Thus, in this study, nitrogen and sulphur co-doped TiO_2/ZnO nanocomposites were developed using a sol-gel method and the effect of calcination temperature (400oC - 800oC) on the chemical properties of TiO_2/ZnO-N, S nanocomposites was determined using X-ray diffraction (XRD), Field Emission Scanning Electron Microscopy (FESEM), and UV-visible spectroscopy. Based on the results, calcination temperature at 600oC gave the optimum characteristic of the catalyst and gave the highest photocatalytic efficiency. At 600oC, the mesoporous structure of TiO_2/ZnO-N,S was obtained with crystallite size of 15.6nm, 35.6% crystallinity, 22.81m2/g surface area and dense layer with less agglomeration on the surface. For optical properties, doping of nitrogen and sulphur into TiO_2/ ZnO able to narrow the band gap to 2.89eV. The kinetic studies of the reaction were studied with Langmuir, Freundlich and Langmuir-Hinshelwood (L-H) models. All the models were compared based on their R2 value and Langmuir adsorption equilibrium constant (Kads) to elucidate the optimum model for the photocatalytic reaction. The result show that the L-H model fitted better to the adsorption, and considered to follow pseudo first-order decay kinetics. The research seeks to provide insights into the design and development of efficient photocatalysts for environmental remediation applications.

Keywords: Calcination, kinetic, nanocomposite, sol – gel, temperature, TiO_2, ZnO

1. INTRODUCTION

Photocatalysis is a promising, ecologically benign method for converting solar energy to chemical energy or chemical conversion over a metal oxide nanostructure, such as the breakdown of pollutants and the production of hydrogen [1]. Due to their tremendous potential for the photocatalytic oxidation of organic contaminants, metal oxide nanostructures like TiO_2, ZnO, CeO_2, and SnO_2 have garnered a significant deal of study attention.

* Corresponding authors: fazlena@uitm.edu.my

Due to its great stability, photocatalytic activity, non-toxicity, and biocompatibility in comparison to other metal oxide nanostructures, ZnO and TiO_2 has received attention [2]. Stefańska *et al*., [3] also reported that ZnO and TiO_2 possess high chemical stability, non-toxic, resistance to chemical breakdown and compatible with each other. However, due to its broad band gap, titanium dioxide (TiO_2) and ZnO (Eg≈ 3.2 eV for crystalline TiO_2 anatase phase and for pure ZnO), high photoactivity can only occur under ultraviolet light (λ<387 nm)[4]. Therefore, several approaches have been proposed to shift the absorption edge of the photocatalysts towards visible light by using hybrid semiconductors (TiO_2/ ZnO, TiO_2/ SiO_2 etc.) and introducing metal and non-metal dopants into their lattices [5] [6]. Some of the dopants that had been studied in the past year are nitrogen (N), iron (Fe), sulphur (S), silver (Ag), phosphorus (P), carbon (C) and others which are able to increase the photocatalytic activity of TiO_2 and ZnO [6][3][7]. To date, TiO_2 and ZnO-based photocatalysts have been co-doped with more than one type of elements, in which able to further increase their photocatalytic activity. Co-doping with non-metallic elements like sulphur (S) and nitrogen (N) is one promising strategy and possible to replace conventionally doped or metal based TiO_2 photocatalysts with these materials. According to Muhamad [8], addition of metal dopants may result in thermal instability of photocatalysts. Furthermore, the process requires an expensive ion-implantation facility and not feasible at a large scale. Thus, non-metal co-dopants of nitrogen and sulphur was chosen in this study. Nitrogen was chosen as a dopant because it has high visible light sensitivity while sulphur able to increase photoactivity of TiO_2 based on previous studies [9]. In the band gap, n-doping introduces new energy levels that enable visible light absorption and lower the band gap energy. According to Cheng *et al*. [10], who investigated how the photoelectric characteristics of Nb, N doped TiO_2 altered over time, the lattice parameters varied in their degree of change as a result of the addition of impurities. The band gap of N-doped TiO_2 was lowered after doping, and the absorption edge of TiO_2's absorption spectrum moved towards visible light. By serving as an electron acceptor, electron-acceptor S-doping promotes charge separation and avoids electron-hole recombination. Due to its ion's ability to show an oxidation state ranging from S^{2+} to S^{6+}, the S atom has been explored as the best non-metal alternative for the decrease of band gap energy (E_g) from TiO_2. Sulphur as an impurity can be incorporated into the TiO_2 structure in either an interstitial or a substitutional position. Therefore, when substitutional doping is taken into account, sulphur might replace titanium or oxygen. According to studies, S^{2+} is found at oxygen sites for anionic doping whereas S^{4+} or S^{6+} can occupy Ti sites for cationic doping [11]. By considering the role of N and S in co-doping to TiO_2, the photocatalytic performance of TiO_2/ZnO are predicted to be improved by combined N and S co-doping.

TiO_2-based and ZnO-based photocatalyst, can be prepared by precipitation, sol-gel or thermal (hydrothermal and solvothermal) method [12][13][11][14]. However, sol-gel method is favourable as compared to other methods because of the ability to produce of homogeneous mixing of dopant, controlled nanoparticle formation, precise control over the stoichiometry of the nanoparticle, high thermal stability, versatile and adaptable to the synthesis of a wide range of materials, high purity product at low temperature and low contaminant, scalability and precise tuning of photocatalytic activities [15]. One of the factors that give significant affect impact to the structural, optical characteristics and function as photocatalysts of these nanocomposites is calcination temperature. Pitkowska *et al*. [14] investigated the effect of different calcination temperatures and nitrogen content levels on the structural characteristics and photocatalytic activity of nanorice-like N-doped TiO_2. The results showed that the photocatalytic activity of the nanorice-like N-doped TiO_2 increased with increasing calcination temperature and nitrogen content. In the study on the effect of calcination temperature on the structure and visible-light photocatalytic activities of (N, S, and C) co-doped TiO_2 nanomaterials, Xuefei *et a.l* [16] found that the photocatalytic activity of the co-doped TiO_2 nanomaterials increased with increasing calcination temperature up to 500 °C, and then decreased at higher temperatures. Similar report has been revealed by Modanlu and Shafiekhani, [17] on their study on the synthesis of pure and C/S/N co-doped titania on Al mesh in photocatalytic of benzene degradation. However, the effect of calcination temperature on the characteristics and photocatalytic performance of TiO_2/ZnO co-

doped with nitrogen and sulphur has not been specifically studied. Thus, thorough understanding of the interactions between co-doping and calcination temperature on the characteristic of TiO_2/ ZnO co-doped with nitrogen and sulphur and its kinetic activities were investigated in this present study. The study aims to elucidate the significant of nitrogen and sulphur co-doping on the chemical and optical characteristics of TiO_2/ZnO and its catalytic properties in photocatalysis reaction that can be beneficial in the catalyst development for environmental and remediation purposes.

2. MATERIAL AND METHODS

2.1 Material

The chemical used in the synthesis of the photocatalyst were Titanium (IV) isopropoxide (97%,) purchased from Sigma Aldrich Corporation, zinc acetate di-hydrate (A.R) from R&M Chemicals, ammonium nitrate (ACS reagent, ≥98%) from Merck Chemical, thiourea (ACS reagent, ≥99%) from Sigma Aldrich Corporation, Ethanol (A.R) from R&M Chemicals and acetic acid (glacial, ≥99.85%) from R&M Chemicals. All chemicals used were analytical grade.

2.2 Synthesis of TiO_2/ ZnO Co-Doped with Nitrogen and Sulphur

Photocatalysts were prepared by using titanium (IV) isopropoxide (TTIP), zinc acetate, ammonium nitrate and thiourea as precursors using sol-gel method. The precursors were weighed based on mass concentration of 1:1:0.5:0.5 of TiO_2: ZnO: N:S respectively. The measured amount of zinc acetate (16 g), thiourea (5.65 g) and ammonium nitrate (2.4 g) were placed inside 90 mL of deionized water and 10 mL of acetic acid. The solution was labelled as Solution A and stirred until all solids were dissolved. Meanwhile, 30 mL of TTIP and 100 mL of ethanol were mixed and marked as Solution B. With steady stirring, Solution A was introduced dropwise into Solution B. The mixture was agitated for an additional 120 minutes at 200 rpm until a visible gel developed. The gel mixture was left for 24 hours to allow the ageing process to take place. After that, the gel was dried at 110 °C until fully dried. The dry gel was crushed and calcined for 3 hours at temperatures ranging from 400 to 800 °C with heating rate of 5 °C/minute. The process is summarized in Figure 1.

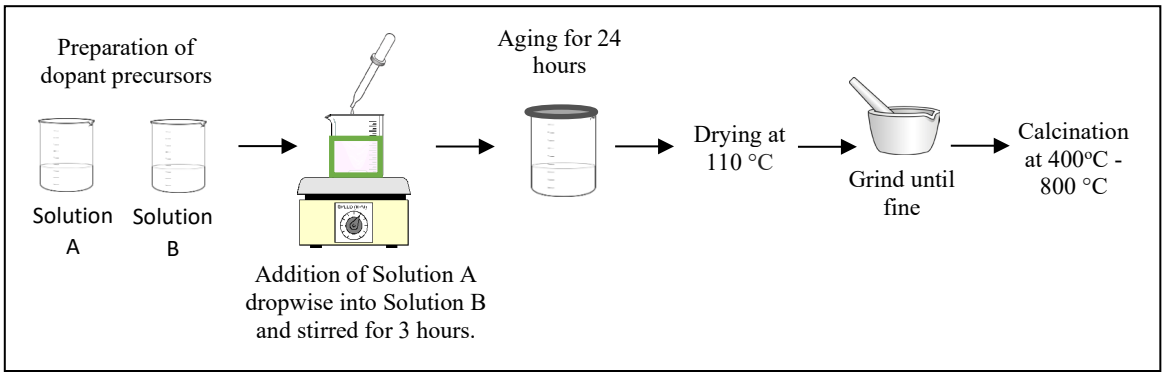

Figure 1. Sol-gel method for synthesis of photocatalyst.

2.3 Characterization of the Developed Photocatalyst

2.3.1 Crystallinity Analysis

The photocatalysts were characterized by using X-Ray Diffractometer (XRD model: Rigaku, D/Max 2200 PC, Japan) with lamp current of 40 mA and power of 40 kW. The analysis was performed at room temperature using copper-Kα radiation (λ=0.15406 nm) with Bragg angles 2θ ranging from 20° to 80° and a scanning rate of 5°/min. The percentage of anatase-rutile of TiO2 were estimated using Equation 1 where I_A and I_R correspond to areas of anatase (101) and rutile (110) respectively.

$$[\mathrm{A}](\%) = \frac{I_\mathrm{A}}{I_\mathrm{A}+1.265I_\mathrm{R}} \times 100 \quad (1)$$

The Debye-Scherrer equation (Equation 2) was used to calculate the crystallite size (D) of photocatalysts, where K is the constant (=0.9), θ is Bragg's diffraction angle, λ is X-ray wavelength (0.1541 nm), and β is full width at half maximum (FWHM) of the diffraction.

$$D = \frac{K\lambda}{\beta\cos\theta} \quad (2)$$

3.2.3 Surface Area and Pore Size Analysis

Brunauer-Emmet-Teller (BET model: Micromeritic ASAP model 2000, USA) was used to study the physical properties of photocatalysts. Before analysis, samples were degassed using nitrogen adsorption-desorption isotherms at -196.15 °C (77 K) for 6 hours. Sample BET specific surface areas were computed using a BET plot in the relative pressure range of $p/p°$=0-1.0. The Barret-Joyner-Halenda (BJH) model was used to calculate pore size and volume.

2.3.3 Surface Morphology Analysis

The morphological study of photocatalysts were carried out by using Field Emission Scanning Electron Microscope (FESEM model: Carl Zeiss, Supra 40VP, Germany) at 5 kV and magnification of 5000 to 30000. Photocatalysts powders were coated with gold in low vacuum.

2.3.4 Optical Properties Analysis

UV-vis Near Infrared Spectroscopy (UV-vis NIR model: Cary 5000 UV-Vis NIR Spectrophotometer, United Kingdom) was used to investigate the optical characteristics of photocatalysts from 200 to 800 nm. Polytetrafluoroethylene (PTFE) was utilised as a reference sample to establish a baseline. The band gap (E_g) of photocatalysts was calculated using the Kubelka-Munk function, which is shown in Equation 3.

$$F(R) = \frac{(1\text{-}R)^2}{2R} = \frac{K}{S} \quad (2)$$

where R is the diffuse reflectance spectra while K and S are absorption coefficient and scattering coefficient respectively. The band gap energy (E_g) was estimated by using the Equation 4.

$$E_\mathrm{g} = \frac{hc}{\lambda} \quad (3)$$

where h is the Plank's constant (4.135667×10^{-15} eV s), c is the velocity of light (3×10^{8} m/s) and λ is the wavelength (nm) of absorption onset.

2.4 Kinetic Study

The photocatalytic activity of photocatalyst was studied by using reactive black 5 (RB5) as model pollutant. The photocatalyst powder was added into 5 mg/L of RB5 and stirred for 30 minutes in dark. The total volume of RB5 solution was set at 100 mL. A 24 W (wavelength ~555nm) compact fluorescent lamp was placed 6 cm from the beakers in a set up photoreactor. The solution was stirred for 5 hours and 5 mL of aliquots was extracted at 30 minutes interval. The aliquots were centrifuged at 10,000 rpm to separate the photocatalyst and the supernatant. The absorbance of RB5 was measured by using UV-Vis Spectrophotometer at 595 nm. The obtained data was plotted using Langmuir, Freundlich and Langmuir-Hinshelwood (L-H) models to determine the kinetic properties of photocatalytic oxidation of RB5. The equations and their linearization forms are described in Equation (2.4) to 7 (Table 1).

Table 1 Adsorption Kinetic Models

Adsorption Model	Equation	Linearize Form
Langmuir	$q_e = \frac{q_{max}.K_{ads}.C_e}{1+K_{ads}.C_e}$ (2.1)	$\frac{1}{q_e} = \frac{1}{K_{ads}.q_{max}}\left(\frac{1}{C_e}\right) + \frac{1}{q_{max}}$ (5)
Freudlich	$q_e = K_F.C_e^{\frac{1}{n}}$ (2.2)	$\ln q_e = \ln K_F + \frac{1}{n}\ln C_e$ (6)
Langmuir-Hinshelwood	$r = \frac{dC}{dt} = \frac{kKC}{1+KC}$ (2.3)	$\ln\left(\frac{C_o}{C}\right) = K_{app}t$ (7)

K_{ads}, K_F and K : adsorption equilibrium constant
C_e and C : concentration of azo dyes at equilibrium (mg/L)
q_e : amount of azo dyes adsorbed on photocatalyst (mg/g)
q_{max} : maximum amount of azo dyes at equilibrium (mg/L)
n : intensity constants of adsorbents
k : reaction rate constants (mg/L min)

3. RESULTS AND DISCUSSION

3.1 Crystallinity Analysis of TiO_2/ ZnO Co-Doped with Nitrogen and Sulphur

The crystallinity of the photocatalysts (TiO_2/ ZnO and TiO_2/ ZnO-N, S) was determined by X-Ray Diffraction (XRD). Figure 2 (a) and (b) illustrate the XRD characteristic peaks for both photocatalysts. The diffraction peaks show the presence of anatase and rutile TiO_2 forms (JCPDS card numbers 21-1272 and 21-1276 for anatase and rutile, respectively).Since there are no trace of brookite phase, the compositions of anatase-rutile form were characterized by using Equation 1 in which IA and IR correspond to areas of anatase (101) at 2θ= 25.5° and rutile (110) at 2θ= 27.7° peaks respectively [18]. The results indicate that the percent of anatase of TiO_2/ ZnO and TiO_2/ ZnO-N, S were 34.8% and 75.3% respectively as tabulated in Table 22. It is known that anatase phase has the highest photocatalytic activity compared to rutile and brookite phase, therefore the co-doping of TiO_2/ ZnO-N, S shows a promising sign in terms of crystallinity [19]. Since the anatase content in TiO_2/ ZnO-N, S was higher than TiO_2/ ZnO it can be said that addition of N and S dopants able to increase the amount of anatase phase in photocatalyst.

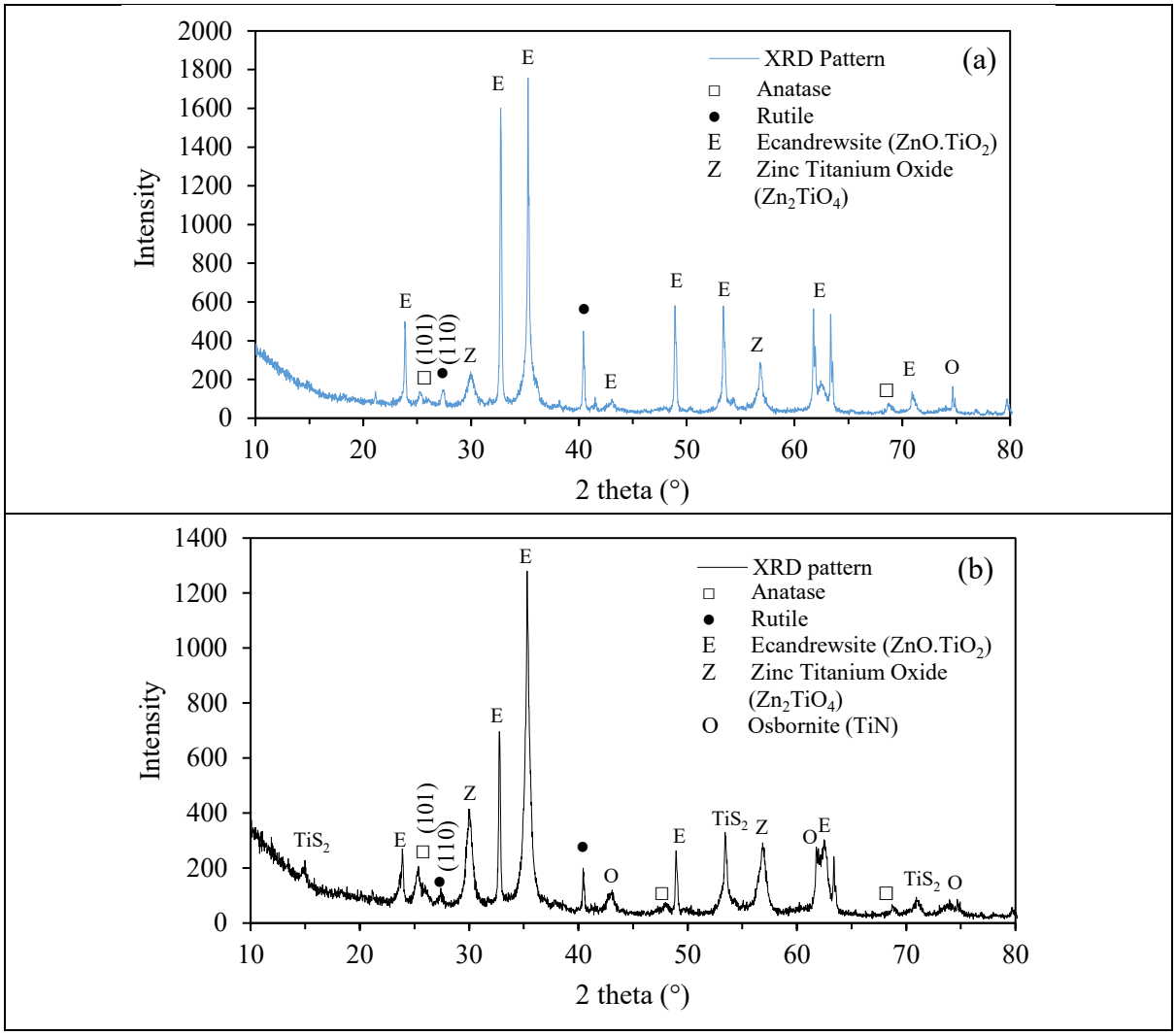

Figure 2. XRD diffraction peaks of (a) TiO_2/ ZnO and (b) TiO_2/ ZnO-N, S at calcination Temperature of 600 °C.

Table 2 XRD Properties of Photocatalysts

Photocatalyst	Phase of Photocatalyst (%)		References
	Anatase	Rutile	
TiO_2 P-25	81.0	19.0	[20]
TiO_2/ ZnO	100	0	[21]
TiO_2/ ZnO	34.8	65.2	This study
TiO_2/ ZnO-N, S	75.3	24.7	This study

The anatase phase of TiO_2/ ZnO and TiO_2/ ZnO-N, S synthesized in this study are lower compared to previous study by Raj & Viswanathan [20] and Cheng *et al*. [21]. Raj & Viswanathan [20] used TiO_2 Degussa (P-25) (commercial form of TiO_2) in the study to determine the transformation of anatase to rutile. It was found out that P-25 has 81% of anatase and the rest is in rutile form. Meanwhile Cheng *et al*. [21] used hydrothermal method and able to produce TiO_2/ ZnO with 100% anatase phase. The result was expected because pure anatase was used as the precursor.

Both photocatalysts have the major characteristic peaks at 2θ = 23.9°, 32.8°, 35.3°, 48.9°, 53.4°, 61.8° and 63.4° which depict cubic zinc titanium oxide ($ZnO.TiO_2$) compound in the form of ecandrewsite (JCPDS card no. 26-1500). Apart from that, there are traces of cubic Zn_2TiO_4 compound in both photocatalysts at peaks 29.8° and 56.5° (JCPDS card no. 25-1164). The presence of Zn_2TiO_4 compound proved that Ti atoms had partially replaced the Zn atoms in Zn crystal lattice [22]. From past literature, addition of N-dopant into semiconductor results in formation of $TiO_{2-x}N_x$ or $Ti_{1-y}O_{2-x}N_{x+y}$ (x = 0.36; y = 0.27) [23]. Similar result was revealed in the present study where titanium nitride (TiN, osbornite-type) was detected at diffraction peaks of 42.63°, 61.89° and 74.13° based on JCPDS card no. 031-1403. This indicates the traces of N in the TiO_2/ ZnO-N, S photocatalyst. According to Zukalova *et al*. [24], TiO_xN_y can be mismatched to TiN because the cubic form seem to be questionable and there are no sufficient research able to justify the formation of TiN at temperature ≥ 600 °C. The argument was further supported by Samiee & Luo [25] in which TiN exhibits similar character with TiO_xN_y and can be mistakenly characterized during nitridation process. The formation of TiN usually happens after calcination at high temperature (more than 1000 °C) in the presence of ammonium gas.

The XRD diffraction peak of TiO_2/ ZnO-N, S shows the presence of titanium disulfide or TiS_2 identical with JCPDS card no. 74-1141 at diffraction peaks of 15.44°, 53.64° and 72.12°. The formation of TiS_2 indicates sulphur was successfully oxidized into TiO_2 lattice [26]. The presence of TiS_2 in the diffraction peak suggested that S^{6+} cation replaces Ti^{4+} ions in the TiO_2 lattice. The peak of TiS_2 in Figure (a) is not as distinctive as compared to TiN peak. According to Rehman *et al*. [27], sulphur has larger ionic radius (1.8 Å for S^{2-}) compared to nitrogen making the insertion of sulphur into TiO_2 lattice more difficult. The result of this issue is the diffraction peaks attributed to TiS_2 is smaller compared to other peaks in Figure 2 (b). The XRD analysis was performed to analyse the crystallinity properties of TiO_2/ZnO-N, S photocatalyst calcined at temperature from 400 to 800 °C and their diffraction peaks are shown in Figure 3 From the intensity and narrowing of the diffraction peaks, it can be seen clearly that the crystallinity of photocatalysts increased along with the calcination temperature. The percentage of crystallinity were tabulated in Table 3 by considering the area under the graph of both crystals and amorphous phase of diffraction peaks. Temperature 400 °C has the lowest crystallinity compared to other temperatures. Some organic molecules might remain in the lattices of 400 °C which causing incomplete crystallization [28].

The diffraction peaks also indicate anatase phase was fully formed at temperature of 400 °C and 500 °C. However, at temperature 600 °C onwards rutile phase started to form in the photocatalysts lattices. The result is similar to TiO_2-N synthesized by Yu *et al*. [29] where rutile phase started to form at temperature 600 °C. Meanwhile, at temperature 800 °C showed 100 % of rutile phase due lacking anatase characteristic peaks. This phase behaviour obtained in the current study follow the composite phase diagram of the TiO_2 as reported by Nie *et al*. [30]. Similar results were obtained from Dodoo-Arhin et al. [31] in which the amount of rutile phase increased as the calcination temperature increased around temperature between 450 °C to 600 °C. The temperature varies with the methods of synthesis and type of precursors used. Based on the diffraction peaks, formation of TiS_2 and TiN can be observed at temperature above 600 °C based on diffraction peaks of 15.44°, 53.64° and 72.12° (JCPDS card no. 74-1141) and 42.63°, 61.89° and 74.13° (JCPDS card no. 031-1403) respectively. Similar temperature for formation of TiS_2 was obtained by Let *et al*. [32], in which formation of TiS_2 started at calcination temperature of 600 °C.

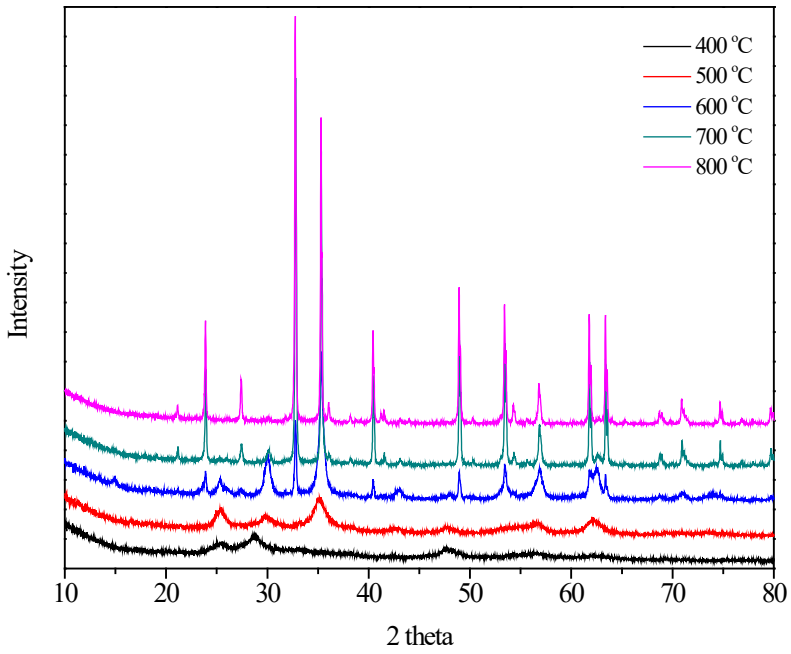

Figure 3. XRD patterns for TiO_2/ ZnO-N, S photocatalyst at different calcination temperature, * depict the main peak for TiS_2 at 15.44°, 53.64° and 72.12°.

Table 3 XRD Properties of Photocatalysts at Different Calcination Temperature

Calcination Temperature (°C)	Crystallinity (%)	Phase of Photocatalyst (%)	
		Anatase	Rutile
400	25.9	100	–
500	35.4	100	–
600	35.6	75.3	24.6
700	35.8	28.1	71.9
800	38.2	–	100

3.2 Crystallite Size Analysis

The average crystallite size in Table 4 was obtained from the XRD patterns of photocatalysts by using Debye-Scherrer's equation (Equation 2) of the main diffraction peaks at 2θ= 35.3°. The size of crystallite was compared with the size of TiO_2 Degussa (P-25) from literature which is 26.0 nm [20]. From the equation, the crystallite sizes (D) of both photocatalysts are 48.2 and 15.6 nm for TiO_2/ ZnO and TiO_2/ ZnO-N, S respectively. TiO_2/ ZnO has larger crystallite size could be associated with the more amount of rutile phase compared to TiO_2/ ZnO-N, S. Rutile phase has larger grain size compared to anatase phase [19]. Furthermore, co-doping of photocatalyst with anionic dopants such as N and S able to influence the size of crystallite. This theory is proven because TiO_2/ ZnO-N, S has smaller crystallite size compared to P-25 and TiO_2/ZnO. According to Sathish et al., [33], N^{3-} and S^{2-} have higher atomic radius than O^{2-} and able to increase the inter planar distance subsequently decrease the "*d*" space values. This can be seen clearly in Figure(b) which shows clear broadening at the highest intensity characteristic peak at 2θ= 35.3°. Similar result was obtained from synthesis of TiO_2-N, S in which the size of crystallite was 20 nm compared to pure TiO_2 which had the size of 24 nm.

Table 4 Crystallite Size of Photocatalysts calcined at 600°C

Photocatalysts	Crystallite Size (nm)	References
P-25	21.0	[20]
TiO_2/ ZnO	48.2	This study
TiO_2/ ZnO-N, S	15.6	This study

The effect of calcination temperature towards TiO_2/ ZnO-N, S were investigated from temperature of 400 to 800 °C. Table 5 summarized the crystallite size of TiO_2/ ZnO-N, S photocatalyst at different calcination temperature. It was found out that the crystallite size increased proportionally with increasing of calcination temperature. The result was supported with previous literature in which calcination temperature will affect the size of crystallite [33]. According to Baharudin *et al*. [34], the increased of size is because of crystallization of photocatalysts and agglomeration of particles due to collapse of mesoporous structure. The increased of crystallite size will further distrupt the surface area of photocatalysts and reduce their effciency.

Table 5 Crystallite Size of TiO_2/ ZnO-N, S at Different Calcination Temperature

Calcination Temperature (°C)	Crystallite Size (nm)
400	4.0
500	5.8
600	15.6
700	48.3
800	50.3

3.3 Surface Area Analysis and Pore Size Distribution Analysis

The surface area of photocatalysts was determined using the Brunauer-Emmett-Teller (BET) method, which involved N2 adsorption and desorption at 77.3 K. Table 6 summarises the features of photocatalysts. From the BET analysis, the surface area of photocatalysts were reduced significantly after doping. The reduction of specific surface area could be associated with increasing of crystallinity of semiconducting oxides [35]. The rutile phase has lower BET surface area and TiO_2/ ZnO has the most amount of rutile in the photocatalyst according to Table 2 The significant reduction also can be resulted by particle-particle interaction of samples or agglomeration. The outcome nature of photocatalyst was influenced by its preparation method. The crucial part of preparation is the hydrolysis stage in which precursors were added with water and acidifying reagent to facilitate the process. Glacial acetic acid (GAA) served as a good acidifying reagent and provide the highest surface area based on previous study. Incomplete hydrolysis may cause the aggregation of particles due to the rapid nature of the process. Since GAA was used in this study, the ratio of solvent and water were probably the source of problem. According to Bashiri *et. al* [28], higher amount of water promotes nucleophilic attack on titania precursor and results in agglomeration of particles.

Table 6 Surface Area and Pore Characteristics of Photocatalysts calcined at 600°C

Photocatalysts	Surface area (m^2/g)	Total pore volume (cm^3/g)	Mean pore diameter (nm)	References
P-25	56.0	0.25	17.5	[20]
TiO_2-N, S	39.5	0.15	8.98	[36]
TiO_2/ ZnO	16.76	0.11	25.0	This study
TiO_2/ ZnO-N, S	22.81	0.15	27.6	This study

Figure 3 shows the adsorption-desorption isotherms for TiO_2/ ZnO and TiO_2/ ZnO-N, S photocatalysts. The isotherms can be classified as type IV according to IUPAC classification for adsorption isotherm which belong to mesoporous materials (pores diameter is between 2–50 nm). The loops of the adsorption-desorption isotherms attributed to type H1 which is well defined cylindrical pore channels. Similar result was obtained by Syafiuddin *et al*. [36] who synthesized TiO_2-N, S as his study. He suggested that the mesoporous region indicates uniform pores and considered as a good photocatalyst. Further doping lessens the pore volume shown by TiO_2/ ZnO-N, S in Table 6 compared to the pore volume of P-25. Similar results can be compared with Yu *et al*. [35] in which doping with other anionic dopants will result in slight reducing of pore volume. The differences of pore volume of photocatalysts were not significantly different and comparable to the closest synthesized photocatalyst by Syafiuddin *et al*. [36]. In his study, the total pore volume of TiO_2-N, S was 0.15 cm3/g. The pore diameters were obtained from Barret–Joyner–Halenda (BJH) method. From the pore distribution data, it was found out that the average size of pore diameter of TiO_2/ ZnO-N, S increased significantly from 17.5 nm (P-25) to 27.6 nm. The pore diameters of photocatalysts were larger compared to previous literature where mostly have diameter less than 10 nm [36]. However, since the pore diameters still belong as mesoporous materials (between 2 and 50 nm), the photocatalysts were acceptable.

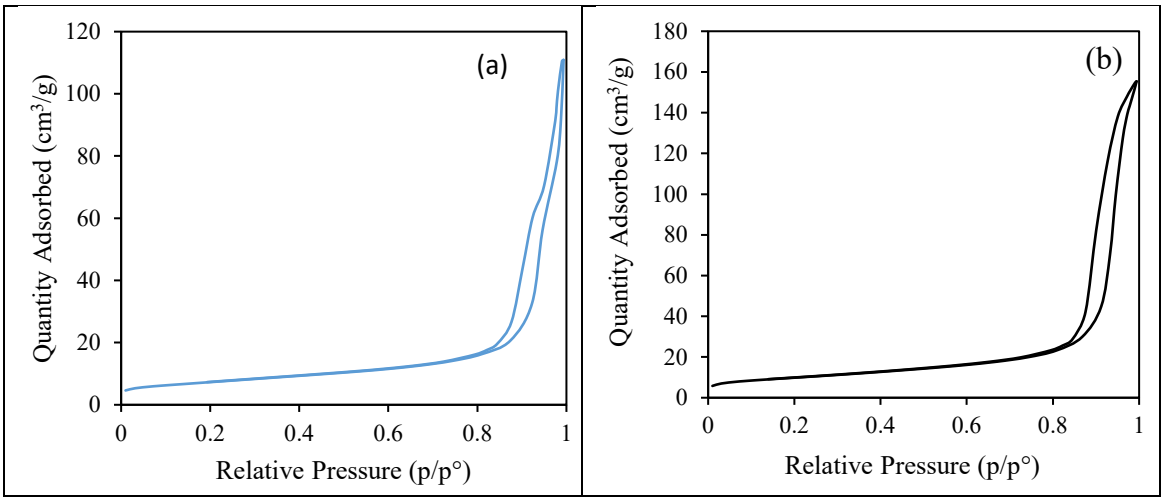

Figure 3. Adsorption-desorption isotherms of (a) TiO_2/ ZnO and (b) TiO_2/ ZnO-N, S at calcination temperature of 600 °C.

The effect of calcination temperature on the surface area of TiO_2/ ZnO-N, S were investigated and tabulated in Table 7 From the result, it was found out that increasing of calcination temperature had serious effect on reduction of the surface area. The surface area of photocatalyst at temperature 800 °C is the lowest compared to others. At high calcination temperature, photocatalysts are prone to agglomerate and reduce their surface area [34].

Table 7 Surface Area and Pore Characteristics of TiO2/ ZnO-N, S at Different Calcination Temperature

Calcination Temperature (°C)	Surface area (m^2/g)	Total pore volume (cm^3/g)	Mean pore diameter (nm)
400	108.67	0.16	5.8
500	53.57	0.16	12.0
600	22.81	0.15	27.6
700	14.13	0.14	35.5
800	4.326	0.01	12.9

The surface area effect can be seen clearly in the adsorption-desorption isotherms for TiO_2/ ZnO-N, S in Figure 5(a) to (d). From the figure, it can be said that the amount of nitrogen adsorbed reduced gradually after calcination temperature increased. However, at temperature of 800 °C, the photocatalyst showed the least amount of nitrogen adsorbed which explains the low surface area (4.82 m^2/g). The photocatalyst belong to type IV IUPAC classification (mesoporous materials) and approaching type II at temperature of 800 °C. Type II isotherm indicates the material is non-porous. This statement is supported with the low total pore volume shown by photocatalyst at temperature 800 °C. The pattern is similar with a study by Raj & Viswanathan [20] in which P-25 had low surface area after being calcinated at temperature above 700 °C have type II isotherms.

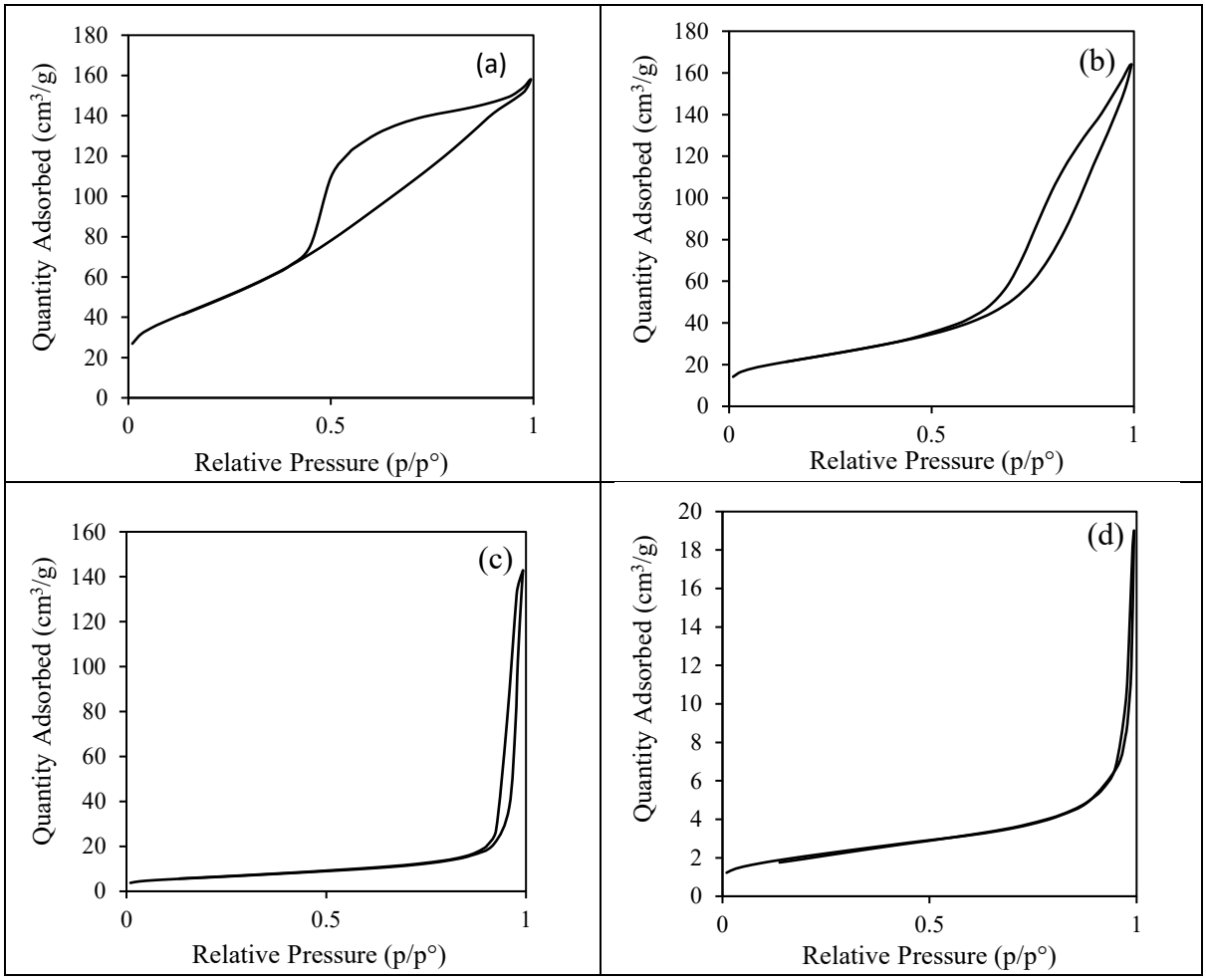

Figure 5. Adsorption-desorption isotherms of TiO_2/ ZnO-N, S at calcination temperature of (a) 400 °C, (b) 500 °C, (c) 700 °C and (d) 800 °C.

The increased of calcination temperature have a serious effect on the pore volume at high temperature. From temperature 400 to 700 °C, only slight reduction of the pore volume occurred. At temperature of 800 °C, the pore volume began to shrink drastically to 0.01 cm^3/g. The reduction of pore volume is because of agglomeration of particles [34]. In contrast, the pore diameter of photocatalyst increased with calcination temperature. However, at temperature of 800 °C, the pore size reduced to 12.9 cm^3/g. It was believed that the mesoporous walls collapse at high temperature due to the agglomeration.

3.4 Surface Morphology Analysis

The surface morphologies of all photocatalysts can be referred by FESEM images in Figure 6. From the image, TiO_2/ ZnO-N, S has dense layer but have lesser agglomeration compared to TiO_2/ ZnO. TiO_2/ ZnO have combination of small spheres and large irregular shapes. There is significant agglomeration in the TiO_2/ZnO particles. Agglomeration is unwanted in any types of photocatalysts because it will subsequently lead to reduction of the surface area and reduce the photoactivity of photocatalyst [37]. The images were supported by the XRD and BET surface area results mentioned in previous sections. TiO_2/ ZnO clearly has larger particle size and lower surface area compared to TiO_2/ ZnO-N, S. The agglomeration seen from the image of TiO_2/ ZnO are proven to be the factor of the low pore volume exhibited by the photocatalyst. The images of photocatalysts are in agreement of a study by Syafiuddin *et al*.[36] in which further doping of TiO_2 able to improve their surface morphologies.

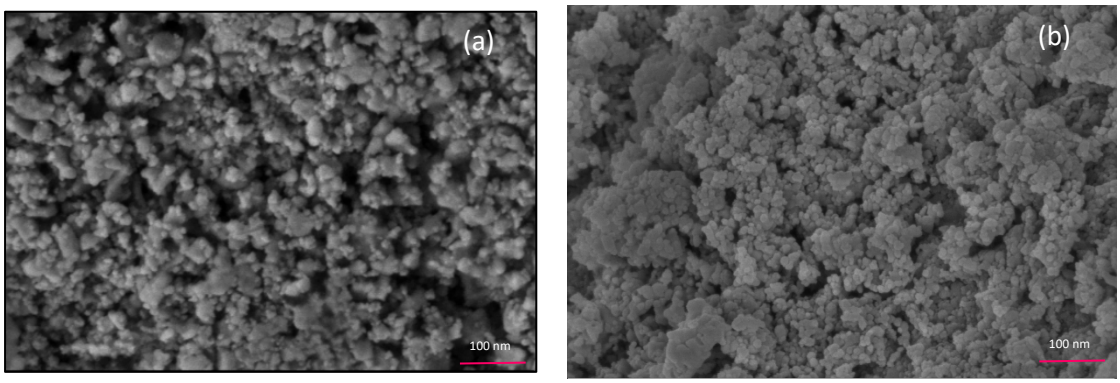

Figure 6. FESEM images for (a) TiO_2/ ZnO and
(b) TiO_2/ ZnO-N, S at calcination temperature of 600 °C (30,000 magnification).

The effect of calcination temperature towards the morphology of TiO_2/ ZnO-N, S photocatalyst is shown in Figure(a) to (e). From the FESEM images, the shapes of particles become less irregular as the temperature increases. At low calcination temperature, the shapes of particles are irregular, and agglomeration occurs at many places. The shapes and agglomeration able to justify the low size of pore diameter shown by Figure 7(a). At low calcination temperature, the thermal energy supplied was unable to cleave the agglomeration into finer entities creating highly clustered particles [37]. According to Bashiri *et al*. [28], low calcination temperature will lead to incomplete crystallization which explains the lack of uniformity of the particles. At temperature of 600 °C, more regular and uniform particles can be seen in the image with the least agglomeration. However, at temperature beyond that the particles tend to agglomerate further, and the shapes and sizes of particles become irregular again which explains the decrease of pore size in previous section. The surface morphology at high calcination temperature able to support the large crystallite size and low surface area that were discussed in previous sections. The agglomeration and large size of crystallite was due to collapse of mesoporous structure of the photocatalyst [34].

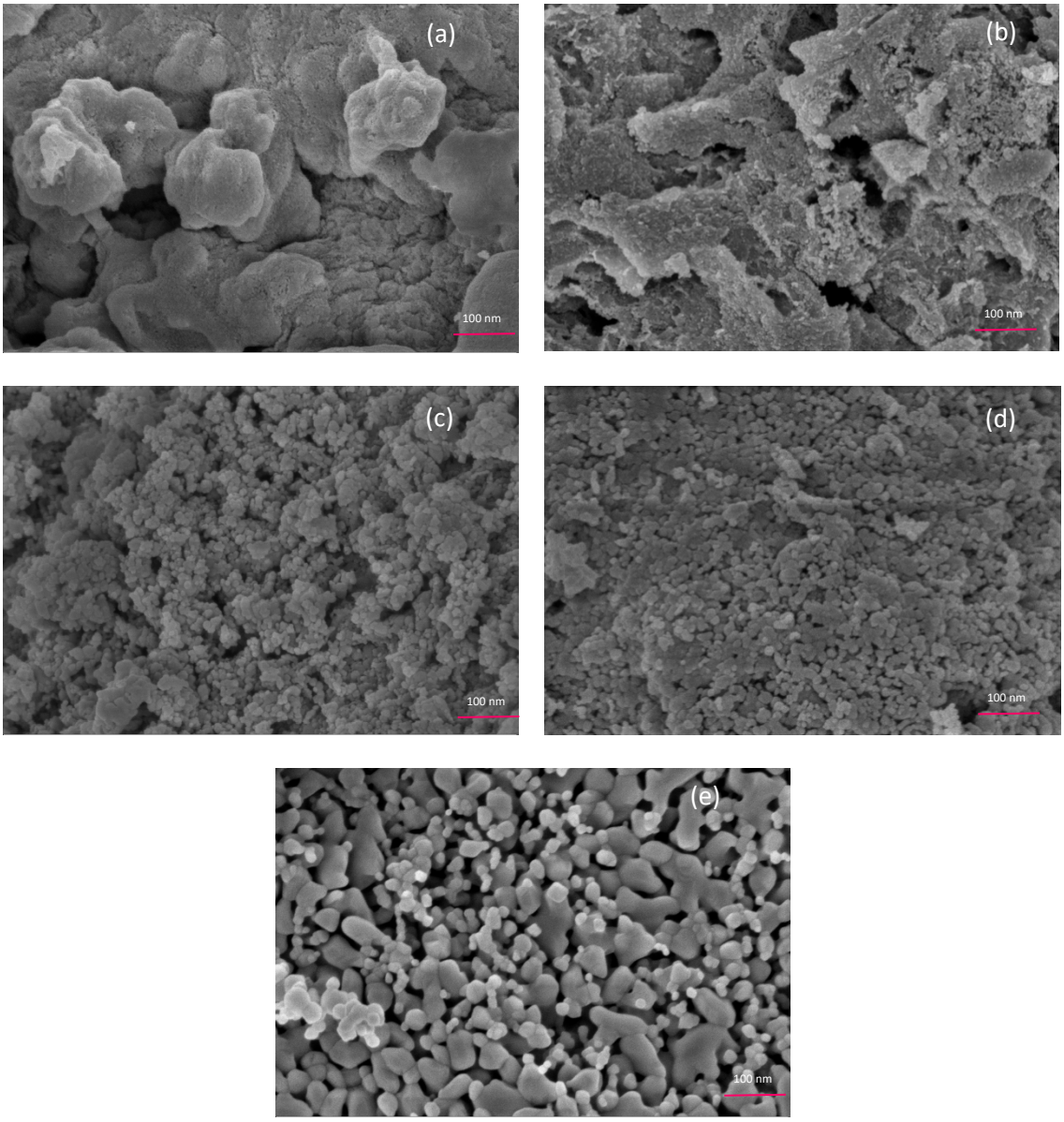

Figure 7. FESEM images of TiO_2/ ZnO-N, S at calcination temperature of (a) 400, (b) 500, (c) 600, (d) 700 and (e) 800 °C (30,000 magnification).

3.5 Energy Band Gap Analysis

The photocatalysts undergo UV-Vis DRS analysis to determine their optical properties. Their diffuse reflectance spectra were translated into a graph of in Figure 8. The wavelength was extrapolated from the plot, and it was found out that the wavelength of TiO_2/ ZnO shifted from 429.3 nm to 426.0 nm after co-doped with nitrogen and sulphur. From Table 8, both photocatalyst have higher wavelength than TiO_2 P-25 and commercial ZnO. Titania and ZnO have a threshold wavelength of 388 nm. The increment of wavelength signifies that the photocatalysts can work under visible light. The direct energy band gap (E_g) of samples was estimated by using Equation 4. From the equation, the energy band gap of each photocatalyst were estimated to be 2.89 eV and 2.91 eV for TiO_2/ ZnO and TiO_2/ ZnO-N, S respectively. Both photocatalysts exhibit lower band gap energies than TiO_2 P-25 and ZnO which is 3.2 eV. From previous studies, the doping of TiO_2 and ZnO able to lower their band gap and approaching visible light region. For instances, Caratto *et al*. [38] and Yu *et al*. [29] able to shift the band gap of TiO_2 to 3.0 eV after doping with nitrogen. On the other hand, Yu *et al*. [35] manage to obtain lower band gap at 2.87 and 2.83 eV

respectively after doping TiO_2 with sulphur via sol-gel method. Co-doping of TiO_2 and ZnO able to shift the band gap ranging between 2.82 to 2.89 eV [39]. As a comparison, this study able to shift 8.4 % and 10 % of TiO_2/ ZnO and TiO_2/ ZnO-N, S respectively from 3.2 eV. From the experiment, it can be said that doping of nitrogen and sulphur into TiO_2/ ZnO able to narrow their band gap and perform better under visible light.

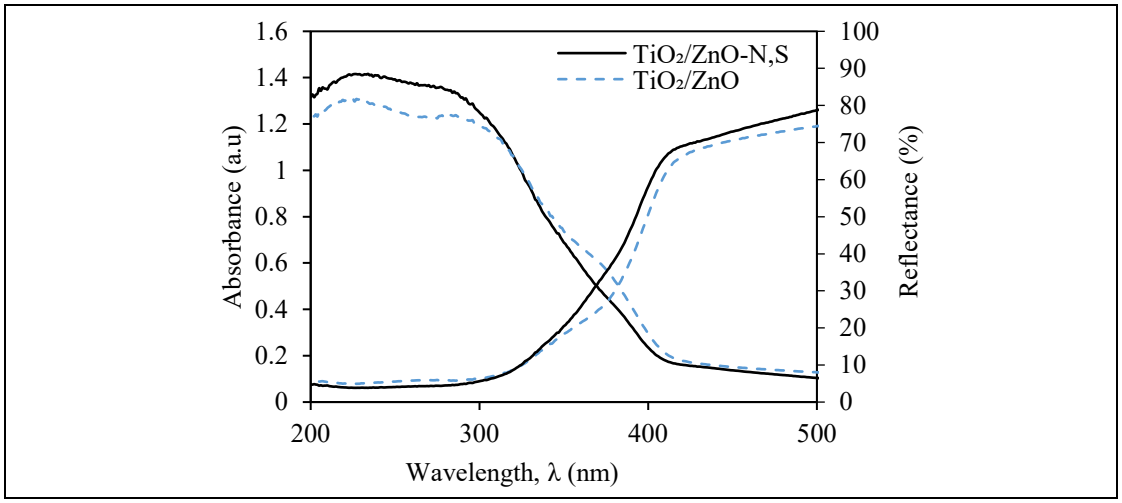

Figure 8. UV-vis reflectance and absorption spectra of TiO_2/ ZnO and TiO_2/ ZnO-N, S at calcination temperature of 600 °C.

Table 8 UV-vis DRS Analysis for Photocatalysts calcined at 600°C

Photocatalyst	UV-vis DRS Analysis		References
	Wavelength (nm)	Band gap (eV)	
TiO_2	400	3.2	[40]
ZnO	387	3.2	[41]
TiO_2/ ZnO	429.3	2.93	This study
TiO_2/ ZnO-N, S	426.0	2.89	This study

The effect of calcination temperature on the wavelength and energy band gap of TiO_2/ ZnO-N, S was investigated. The UV-vis reflectance spectra and Tauc plot of TiO_2/ ZnO-N, S is illustrated in Figure 9.9. The energy band gap of TiO_2/ ZnO-N, S at different calcination temperature was estimated using linearization of Kubelka-Munk function and summarized in Table 9. The energy band gap of the photocatalyst varies from 2.76 to 3.07 eV. From the absorption spectra, the wavelength of photocatalyst decreased with increasing of calcination temperature except for temperature 500 °C. However, the wavelength of temperature 500 °C is not too far off the next temperature. The result is in agreement with Singh *et al*. [42] in which the calcination temperature affect the wavelength of photocatalyst.

Based on a research by Kayani *et al*. [43], the energy band gap is closely related to the size of crystallite as larger crystallite will yield higher band gap. The energy band gap started to rise between temperature of 400 °C and 500 °C from 2.76 to 3.07 eV. The reason is enlargement of crystallite size as discussed earlier. At temperature 600 °C, the band gap decreases significantly to 2.89 eV. Based on the XRD analysis, at this temperature is the starting point of rutile formation. Rutile generally has lower energy band gap compared to anatase phase [20]. The formation of rutile phase able to decrease the energy band gap at this temperature. At temperature 700 and 800 °C, the band gap increased and maintained at around 2.95 eV.

Despite having more rutile phase compared to temperature 600 °C, their crystallite sizes increased from 15.6 nm to 48.3 and 50.3 nm for temperature 700 °C and 800 °C respectively. Therefore, it is understandable for the increased at their energy band gap.

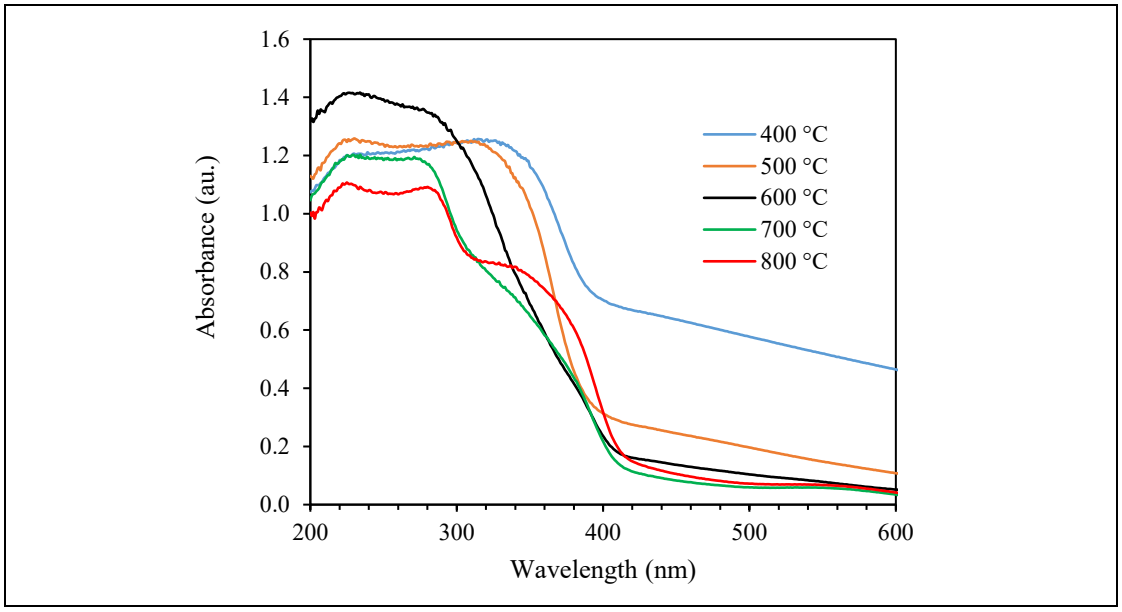

Figure 9. UV-vis reflectance spectra of TiO_2/ ZnO-N, S at different calcination temperature.

Table 9 UV-vis DRS Analysis for TiO_2/ ZnO-N, S at Different Calcination Temperature

Calcination Temperature (°C)	UV-vis DRS Analysis	
	Wavelength (nm)	Band gap (eV)
400	448.6	2.76
500	404.2	3.07
600	429.0	2.89
700	420.5	2.95
800	419.5	2.96

3.6 Kinetic Study

The kinetic studies of the reaction were studied with Langmuir, Freundlich and Langmuir-Hinshelwood (L-H) models. All the models were compared based on their R^2 value. The models are illustrated in Figure 10(a)-(c). The isotherms constants of each model were tabulated in Table 10. From the table, the Langmuir model shows the highest R^2 compared to Freundlich and L-H model. However, the y-intercept which corresponds to the Langmuir adsorption equilibrium constant (K_{ads}) fell into the negative region. Hence, the L-H model fitted better to the adsorption based on similar case reported by Islam *et al*. [44]. The L-H model is used to describe the photocatalytic process and considered to follow pseudo first-order decay kinetics. Figure 10(c) shows the plot of $\ln(C_o/C)$ against time at different initial concentrations. From the plot, the first order rate constant can be determined (K_{app}) by using the slope of the graph and summarized in Table 10. From the table, K_{app} values were reduced compared to initial concentration of 10 mg/L. The results were in agreement by previous literature in which the K_{app} dropped from 0.02 min-1 to 0.007 min-1 as the concentration increases from 2 mg/L to 20 mg/L [45].

The reduction of adsorption at higher concentrations may cause by reduction of available sites on the photocatalyst compared to the amount of RB5 [46]. Furthermore, the concentrations will lower the chance of light passing through and inhibits the formation of hydroxyl radicals needed for the oxidation to occur.

Table 10 Isotherm Model Parameters Based on Effect of Initial Concentration of RB5

Isotherms	Initial Concentration (mg/L)				
	5	10	15	20	25
Langmuir					
Q_m	1.434E-04	4.526E-04	7.366E-04	9.550E-04	1.338E-04
K_{ads}	-0.933	-2.167	-2.865	-1.999	-35.231
R^2	0.987	0.996	0.996	0.990	0.997
Freundlich					
n	-2.106	-8.905	-5.967	-5.855	-9.634
K_F	3.836E-04	6.454E-04	1.069E-03	1.493E-03	1.738E-03
R^2	0.969	0.987	0.949	0.939	0.930
Langmuir-Hinshelwood					
K_{app} ($\times 10^{-3}$ min^{-1})	3.917	2.283	2.150	1.833	2.567
r	0.039	0.046	0.065	0.073	0.128
R^2	0.952	0.913	0.905	0.915	0.936

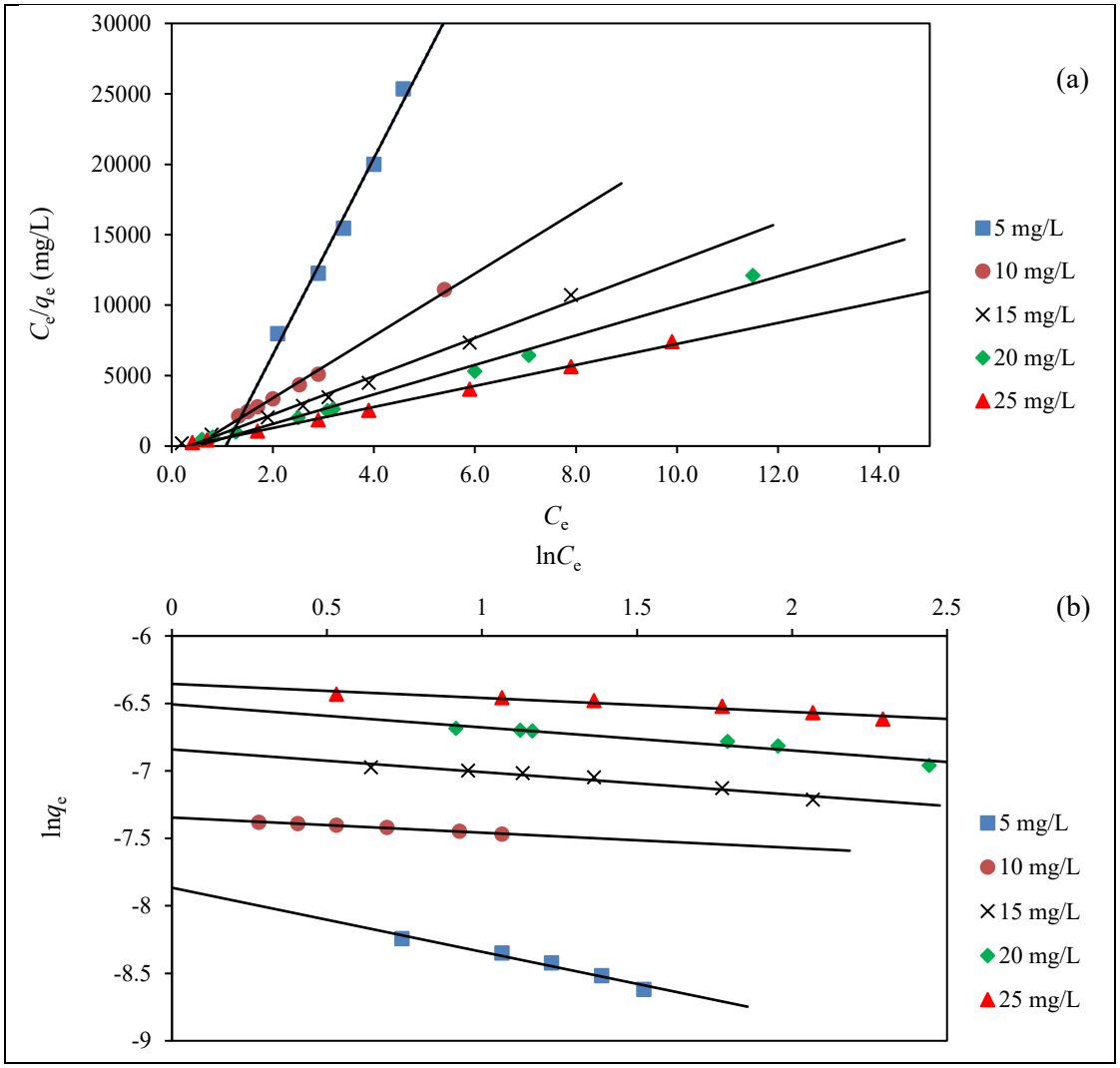

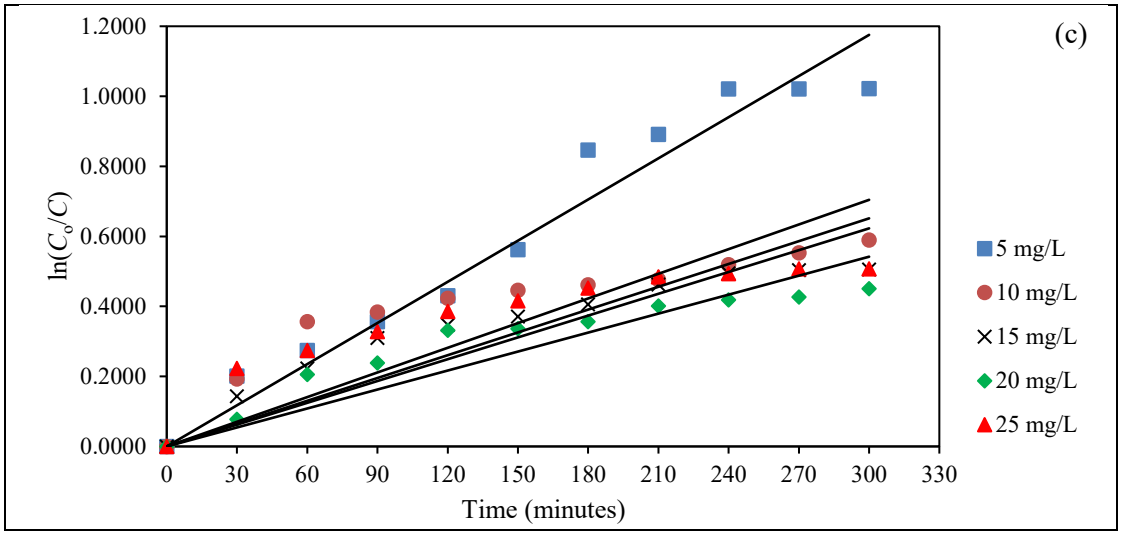

Figure 10. Kinetic studies based on initial concentrations of RB5 using (a) Langmuir, (b) Freundlich and (c) L-H models (Tc=600 °C, Loading=3 g/L, pH 6)

From the kinetic studies, the photocatalytic performance at concentration 5 mg/L exhibit the highest K_{app} (3.917×10^{-3} min^{-1}) than the other concentrations. On the other hand, the reaction rate of reactant (r) increased proportionally with the initial concentration of RB5. The K_{app} of this study is lower compared to another literature by Zhu *et al*. [45] in which the highest K_{app} achieved was 7.03×10^{-3} min^{-1} at 10 mg/L of methyl orange dye solution. However, the conditions of experiments were not similar, therefore higher Kapp was expected from this study.

4. CONCLUSION

The sol-gel method was used to create the photocatalyst TiO_2/ZnO-N, S, which has a good balance of anatase and rutile phases as well as traces of zinc titanium oxide, titanium nitride, and titanium disulfide in its lattice. The findings indicate that the dopants were successfully incorporated into the lattices because TiS_2 and TiN were present as indicated by diffraction peaks at 15.44°, 53.64°, and 72.12° (JCPDS card no. 74-1141) and 42.63°, 61.89°, and 74.13° (JCPDS card no. 031-1403), respectively. As the calcination temperature rises, the size of the crystallites grows, the catalyst's surface area decreases, particles clump together on the developed catalyst's surface, and a band gap (E_g) lower than 3.2 eV is achieved. The calcination temperature of 600°C was the optimum temperature for the production of TiO_2/ZnO-N, S photocatalyst, taking into account surface morphology (less agglomeration), crystallite size (15.6 nm), surface area (22.81 m^2/g), and band gap (2.89 eV). Based on kinetic studies, RB5 at various concentrations (5 mg/L to 25 mg/L) was removed using a TiO_2/ZnO-N, S photocatalyst that was calcined at 600°C showed that the L-H model was best fit by the RB5 removal which was also thought to follow pseudo first-order decay kinetics. With the reactant (r) oxidising at a rate of 0.039 mg/L.min, the apparent deterioration rate of the constant (K_{app}) was 3.917 10^{-3} min^{-1}. The present study revealed that a calcination temperature of 600°C produced TiO_2/ZnO-N, S with the optimum characteristics and the maximum photocatalytic efficiency.

ACKNOWLEDGEMENTS

Author is gratefully acknowledged to Universiti Teknologi MARA (UiTM) for financially and technically supporting this research under 600-RMC/GPK 5/3 (180/2020) and 600-RMC/GPK 5/3 (149/2020). The author also would like to thank College of Engineering and School of Chemical Engineering for the continuous support in the research development and internal fund. A high appreciation to the Malaysia Ministry of Higher Education for the continuous support in academic research.

REFERENCES

[1] Zhengisbek, K., Baglan, B., Alzhan, B., Aidos, I., Mukhtar, Y., Chingis, D., Science of The Total Environment, vol. 885, (2023) pp.163914.
[2] Sadikin, S. N., Ridwan, J., Ali Umar, M. I., Mohd Raub, A. A., Yunas, J., Hamzah, A. A., Dahlan, D., Abd Rahman, M. Y., Ali Umar, A., International Journal of Electrochemical Science, vol.18, issue 9(2023) pp. 100246.
[3] Stefańska, K., Ożegowska, K., Hutchings, G., Popis, M., Moncrieff, L., Dompe, C., Janowicz, K., Pieńkowski, W., Gutaj, P., Shibli, J. A., Prado, W. M., Piotrowska-Kempisty, H., Mozdziak, P., Bruska, M., Zabel, M., Kempisty, B., Nowicki, M., Journal of clinical medicine, vol. 9, issue 4 (2020) pp. 1102.
[4] Muthukrishnan, S., Vidya, R., Sjåstad, A. O, Materials Chemistry and Physics, vol. 299, (2023), pp.127467.
[5] Yunus, N. N., Hamzah, F., So'aib, M. S., Krishnan J., AIP Conf. Proc., vol. 1901, (2017) pp. 100004.
[6] Sikirman, A., Krishnan, J., Mohamad, E. N., Applied Mechanics and Materials, vol. 661, (2014) pp. 34–38.
[7] Mahmood, A., Naeem, A., Recent Applications in Sol-Gel Synthesis, (2017) pp. 169–193.
[8] Teh, C. M., Mohamed, A. R., Journal of Alloys and Compounds, vol. 509, issue 5 (2011) pp. 1648–1660.
[9] Panagiotis,G., Smirniotis, T. B., Devaiah, D., Siva, N. R. I., Catal. Commun., vol. 113, (2018) pp. 1-5.
[10] Cheng, L., Zhang, H. G., Liu, W., Zhao, X. Z., Acta Phys. Sin., vol. 61, issue 23 (2012) pp. 514-518.
[11] Vorontsov, A. V., Valdés, H., Int. J. Hydrogen Energy, vol. 44, (2019) pp. 17963-17973.
[12] Pillai, V. V., Lonkar, S. P., Alhassan, S. M., ACS Omega, vol. 5, (2020) pp. 7969-7978.
[13] da Silva, A. I., Bettini, J., Bernardes, A. A., Castro, R. H. R., Gouvêa, D., J. Phys. Chem. C, vol. 127, (2023) pp. 1536-1547.
[14] Piatkowska, A., Janus, M., Szymanski, K., Mozia C-N-S., Catalyst, vol. 11, (2021) p. 144.
[15] Akpan, U. G., Hameed, B. H., Applied Catalysis A: General, vol. 375, issue 1 (2010) pp. 1–11.
[16] Xuefei, L., Xue, X., Yang, H., Chen, C., Applied Surface Science, vol. 332, (2015).
[17] Modanlu, S., Shafiekhani, Sci Rep, vol. 9, issue 16648 (2019).
[18] Su, R., Bechstein, R., Sø, L., Vang, R. T., Sillassen, M., Esbjörnsson, B., Besenbacher, F., Journal of Physical Chemistry C, vol. 115, issue 49 (2011) pp. 24287–24292.
[19] Hanaor, D. A. H., & Sorrell, C. C., Journal of Materials Science, vol. 46, issue 4(2011), pp. 855–874.
[20] Raj, K. J. A., & Viswanathan, B., Indian Journal of Chemistry, vol. 48, (2009) pp. 1378–1382.
[21] Cheng, C., Amini, A., Zhu, C., Xu, Z., Song, H., Wang, N., Scientific Reports, vol. 4, issue 4181 (2014) pp. 1–5.
[22] Mebrek, A., Alleg, S., Benayache, S., & Benabdslem, M., Ceramics International, vol. 44, (2018) pp. 10921–10928.
[23] Gou, H., Zhang, G., & Chou, K., Journal of Materials Science, vol. 52, issue 3 (2017) pp. 1255–1264.

[24] Zukalova, M., Prochazka, J., Bastl, Z., Duchoslav, J., Rubacek, L., Havlicek, D., Kavan, L. Facile Conversion of Electrospun TiO2 into Titanium Nitride / (2010).
[25] Samiee, M., Luo, J., Journal of Power Sources, vol. 245, (2014) pp. 594–598.
[26] Liu, B., Yang, J., Liu, C., Hu, T., Han, Y., Gao, C., Tis, I., Physica Status Solidi, vol. 1686, issue 5 (2011) pp. 1683–1686.
[27] Rehman, S., Ullah, R., Butt, A. M., & Gohar, N. D., Journal of Hazardous Materials, vol. 170, (2009) pp. 560–569.
[28] Bashiri, R., Mohamed, N. M., Kait, C. F., Recent Applications in Sol-Gel Synthesis, (2017) pp. 151–167.
[29] Yu, H., Zheng, X., Yin, Z., Tao, F., Fang, B., & Hou, K., Chinese Journal of Chemical Engineering, vol. 15, issue 6 (2007) pp.802–807.
[30] Nie, X. L, Zhuo, S. P., Maeng, G., Sohlberg, K., International Journal of Photoenergy, vol. 2009, pp. 1-22.
[31] Dodoo-Arhin, D., Buabeng, F. P., Mwabora, J. M., Amaniampong, P. N., Agbe, H., Nyankson, E., Asiedu, N. Y., Heliyon, vol. 4, issue 7 (2018) pp. 2405 – 8440.
[32] Let, A. L., Mainwaring, D. E., Rix, C. J., & Murugaraj, P., Journal of Physics and Chemistry of Solids, vol. 68, (2007) pp.1428–1435.
[33] Sathish, M., Viswanath, R. P., & Gopinath, C. S., Journal of Nanoscience and Nanotechnology, vol. 9, issue 1 (2009) pp. 423–432.
[34] Baharudin, K. B., Abdullah, N. A., Derawi, D., Materials Research Express, vol. 5, issue 12 (2018) pp. 25018.
[35] Yu, C., Cai, D., Yang, K., Yu, J. C., Zhou, Y., Fan, C., Journal of Physics and Chemistry of Solids, vol. 71, issue 9 (2010) pp. 1337–1343.
[36] Syafiuddin, A., Hadibarata, T., Zon, N. F., Salmiati, Journal of the Chinese Chemical Society, vol. 64, issue 11 (2017) pp. 1333-1339.
[37] Lee, K. M., Lai, C. W., Ngai, K. S., Juan, J. C., Water Research, vol. 88, (2016) pp. 428–448.
[38] Caratto, V., Setti, L., Campodonico, S., Carnasciali, M. M., Journal of Sol-Gel Science and Technology, vol. 63, (2012) pp. 16–22.
[39] Reza, M., Khaki, D., Saleh, M., Aziz, A., Raman, A., Mohd, W., Wan, A., Journal of Molecular Liquids, vol. 258, (2018) pp. 354–365.
[40] Shi, W., Yang, W., Li, Q., Gao, S., Shang, P., Shang, J. K., Nanoscale Research Letters, vol. 7, issue 1 (2012) pp. 590 - 599.
[41] Shifu, C., Wei, Z., Sujuan, Z., Wei, L., Chemical Engineering Journal, vol.148, (2009) pp. 263–269.
[42] Singh, R. P., Hudiara, I. S., Rana, S. B., Materials Science-Poland, vol. 34, issue 2 (2016) pp. 451–459.
[43] Kayani, Z. N., Saleemi, F., Batool, I., Applied Physics A, vol. 119, issue 2 (2015) pp. 713–720.
[44] Islam, M. A., Sakkas, V., Albanis, T., International Journal of Environmental Analytical Chemistry, vol. 90, issue 3-6 (2010) pp. 357–368.
[45] Zhu, H., Jiang, R., Fu, Y., Guan, Y., Yao, J., Xiao, L., Zeng, G., Desalination, vol. 286, (2012) pp. 41–48.
[46] Kilic, M., Apaydin-Varol, E., Pütün, A. E., Journal of Hazardous Materials, vol. 189, issue 1-2 (2011) pp. 397–403.